JCTC Journal of Chemical Theory and Computation

pubs.acs.org/JCTC Article

Perturbative Coordinate Descent Full Configuration Interaction

Zhenlin Zhang,[‖] Mingyu Qiu,[‖] Yingzhou Li,[*] and Wei Hu[*]

Cite This: *J. Chem. Theory Comput.* 2026, 22, 5005−5019 Read Online

ACCESS | Metrics & More | Article Recommendations

ABSTRACT: The coordinate descent full configuration interaction (CDFCI) is an accurate and efficient method for calculating ground-state energies of molecular systems. In this work we introduce two perturbative extensions of original CDFCI. We first propose a direct CDFCI + PT to further correct variational energy by perturbation theory. We also propose an iterative perturbative CDFCI (IP-CDFCI) to avoid evaluating the overlarge perturbative space and catch the information encoded in variational stage. In IP-CDFCI, we store three sparse vectors in a Hash table: $\boldsymbol{c}$, $\boldsymbol{b}$ and $\boldsymbol{d}$, where $\boldsymbol{c}$ is the variational wave function, $\boldsymbol{b}$ is the compressed approximation of $H\boldsymbol{c}$ and $\boldsymbol{d}$ is the perturbative wave function, respectively. By utilizing the redundant memory in the storage of $\boldsymbol{c}$, we can calculate perturbation without any extra memory compared to original CDFCI. We also use a strategy to eliminate the expensive repetitive evaluation of diagonal elements of Hamiltonian by creating a vector $\boldsymbol{h}$ which stores the diagonal entries of Hamiltonian. This strategy trades memory usage for computational time and reduces the computing time significantly. Furthermore, we use quadruple-precision floating-point numbers to improve the numerical stability of perturbative energy. We demonstrate the effectiveness of the single-threaded IP-CDFCI and the multithreaded CDFCI + PT, respectively, by performing calculations on several small molecular benchmarks as well as challenging correlated system: the chromium dimer.

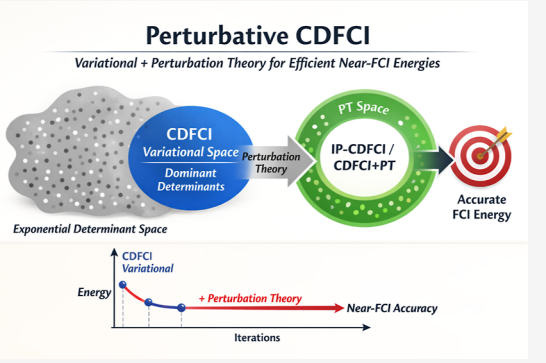

1. INTRODUCTION

Full configuration interaction (FCI) is a highly accurate quantum chemical method that provides the exact solution to the nonrelativistic electronic Schrödinger equation within a finite basis set.[1−3] It yields exact eigenstates and eigenvalues of the Hamiltonian operator, which represents the total energy of the system.[4,5] FCI is capable of describing both static and dynamic correlation effects and can treat systems that are beyond the reach of conventional single-reference approaches. However, the method suffers from factorial scaling of the determinant space, making it impractical for anything but the smallest systems.

To alleviate this computational bottleneck, numerous reduced-scaling FCI variants have been developed. Among these, selected configuration interaction (SCI) methods form a widely used class.[6−10] SCI restricts the variational space to a subset of Slater determinants that contribute most significantly to the total energy, thus capturing the dominant static correlation while discarding many determinants responsible for dynamic correlation.

The semistochastic heat-bath CI (SHCI) method[11−13] is a particularly efficient SCI algorithm that accelerates determinant selection through a heat-bath criterion and applies a stochastic perturbative correction inspired by FCIQMC.[14] More recently, the coordinate-descent FCI (CDFCI) method[15−18] has been introduced, which iteratively updates determinant coefficients via coordinate-descent optimization, compresses determinants with small amplitudes, and uses their visiting frequency as an importance indicator. CDFCI can be viewed as a continuous-optimization analogue of SCI, balancing accuracy and memory efficiency.

Since truncating the determinant space introduces an energy error, most SCI workflows apply second-order perturbation theory (PT) to recover the missing dynamic correlation.[6,19] Beyond SCI + PT, other iterative approaches include the density matrix renormalization group (DMRG)[20−22] and FCI quantum Monte Carlo (FCIQMC),[23−26] which can capture both static and dynamic correlation when the variational space is sufficiently large or adaptively expanded, although the eigenvalue problem becomes increasingly challenging.

In this work, we introduce an extension of original CDFCI named coordinate descent full configuration interaction plus perturbation theory (CDFCI + PT), which is similar to traditional SCI + PT method and a new method called iterative perturbative coordinate descent full configuration interaction

Received: January 20, 2026
Revised: April 20, 2026
Accepted: April 23, 2026
Published: May 7, 2026

https://doi.org/10.1021/acs.jctc.6c00103
J. Chem. Theory Comput. 2026, 22, 5005−5019

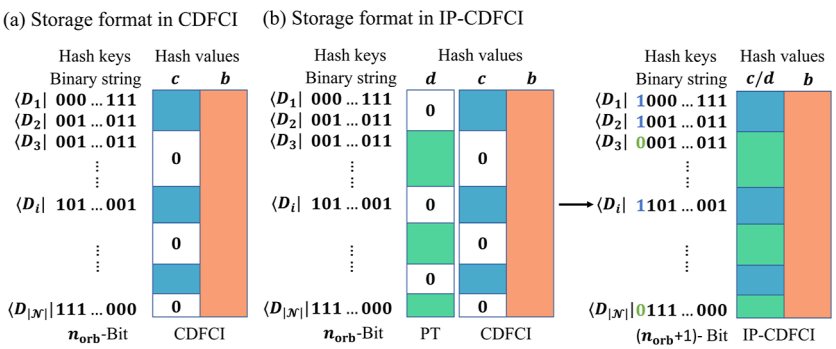

Figure 1. A schematic representation of the main storage of sparse vectors $\boldsymbol{c}$, $\boldsymbol{b}$ and $\boldsymbol{d}$ in our algorithms, which correspond to the variational wave function coefficient vector, the compressed sparse vector $H\boldsymbol{c}$, and the perturbative wave function coefficient vector. The stored elements include all nonzero elements of the sparse vector $\boldsymbol{b}$, indicated by the orange region in the diagrams. (a) The storage of sparse vectors $\boldsymbol{c}$ and $\boldsymbol{b}$ in the standard CDFCI algorithm. Nonzero elements of the sparse vector $\boldsymbol{c}$ are represented by the blue region. The binary strings represent Slater determinants that require n_{orb} bits to represent. (b) The storage of sparse vectors $\boldsymbol{c}$, $\boldsymbol{b}$ and $\boldsymbol{d}$ in IP-CDFCI algorithm. Nonzero elements of the sparse vector $\boldsymbol{d}$ are represented by the green region. The left figure illustrates the orthogonal relationship between perturbative vector $\boldsymbol{d}$ and variational vector $\boldsymbol{c}$ in the standard CDFCI algorithm. The right figure shows the storage of $\boldsymbol{c}$ and $\boldsymbol{d}$ together in the IP-CDFCI algorithm. It uses a binary string to distinguish the ownership of vector elements, with an additional bit added to the highest position of the binary string.

(IP-CDFCI), which takes advantage of the iterative feature of CDFCI and embeds the perturbative correction into the variational iteration. The new variational plus perturbative energy in each iteration often converges faster in the benchmarks considered here than the original CDFCI. Compared with standard SCI + PT workflows, the present implementation introduces only limited and controllable memory overhead within the selected compressed space.

In Section 2, we review the algorithm skeleton of the original variational CDFCI. In Section 3, we present our two new perturbative CDFCI algorithms, which does not introduce any extra memory cost from the original CDFCI. In Section 4, we provide implementation details for perturbative calculations. In Section 5, we present benchmarks of our perturbative CDFCI methods.

2. VARIATIONAL COORDINATE-DESCENT FCI

The many-body Hamiltonian in second-quantization is given by

$$\hat{H} = \sum_{pq} t_{pq}\hat{a}_p^\dagger \hat{a}_q + \frac{1}{2}\sum_{prqs} v_{prqs}\hat{a}_p^\dagger \hat{a}_r^\dagger \hat{a}_q \hat{a}_s \tag{1}$$

In FCI calculations, the ground state wave function is described by the space spanned by all the N-particle Slater determinants that is a subspace of the total Fock space. The time-independent Schrödinger equation can be represented as a matrix equation

$$H\boldsymbol{c} = E_0\boldsymbol{c} \tag{2}$$

In FCI problem the Hamiltonian matrix $H \in \mathbb{R}^{N_{\text{FCI}}\times N_{\text{FCI}}}$ and the coefficient vector of ground state wave function $\boldsymbol{c} \in \mathbb{R}^{N_{\text{FCI}}}$. We know from the second-quantization formula that the Hamiltonian matrix $H_{ij} = \langle D_i|\hat{H}|D_j\rangle$ is nonzero only if $|D_i\rangle$ can be obtained from $|D_j\rangle$ via changing at most two occupied states. We say that $|D_i\rangle$ is H-connected with $|D_j\rangle$ if H_{ij} is nonzero. We denote the H-connected index set of $|D_j\rangle$ as $\mathcal{I}_H(j)$.

CDFCI[27−30] first reformulates the FCI eigenvalue problem as an unconstrained nonconvex optimization problem

$$\min_{\boldsymbol{c}\in\mathbb{R}^{N_{\text{FCI}}}} f(\boldsymbol{c}) = \|H + \boldsymbol{c}\boldsymbol{c}^{\mathrm{T}}\|_F^2 \tag{3}$$

where $\|\cdot\|_F$ denotes the Frobenius norm, and the gradient of the objective function is

$$\nabla f(\boldsymbol{c}) = 4H\boldsymbol{c} + 4(\boldsymbol{c}^{\mathrm{T}}\boldsymbol{c})\boldsymbol{c} \tag{4}$$

The nontrivial stationary points of the gradient of the objective function $f(\boldsymbol{c})$ correspond to the scaled eigenvectors of the Hamiltonian matrix H. Among these stationary points, the scaled ground-state eigenvector of H is the local minimizer of $f(\boldsymbol{c})$, and all other scaled excited-state eigenvectors are saddle points. Notably, the local minimizer corresponding to the ground state has the unique minimum value of the objective function, and thus is also the global minimizer of $f(\boldsymbol{c})$.

The CDFCI algorithm stores the nonzero elements of two sparse vectors, $\boldsymbol{c}^{(l)}$, $\boldsymbol{b}^{(l)} \in \mathbb{R}^{N_{\text{FCI}}}$, in the main memory, which are contiguously maintained throughout iterations. $\boldsymbol{c}^{(l)}$ is the current coefficient vector of the ground state wave function in the l-th iteration, while $\boldsymbol{b}^{(l)}$ is a compressed approximation of $H\boldsymbol{c}^{(l)}$. We denote $\text{supp}(\cdot)$ as the nonzero index of a vector. For example, for a sparse vector $\boldsymbol{a}$

$$\text{supp}(\boldsymbol{a}) = \{j|a_j \neq 0\} \tag{5}$$

Hence, $\text{supp}(\boldsymbol{c}^{(l)})$ is the variational space, and $\text{supp}(\boldsymbol{b}^{(l)})$ is a compressed space connected to the variational space in the l-th iteration. The cardinality of $\text{supp}(\boldsymbol{b}^{(l)})$ can increase drastically and cause memory explosion, so compression technology must be used to control the upsurge of $\text{supp}(\boldsymbol{b}^{(l)})$ and mainly work on the space of $\text{supp}(\boldsymbol{b}^{(l)})$ for variational or perturbative calculation. We expect at large iteration number the space of $\text{supp}(\boldsymbol{b}^{(l)})$ is same as N-particle Hilbert space. We use $\mathcal{N}^{(l)}$, $\mathcal{V}^{(l)}$ and $\mathcal{P}^{(l)}$ to represent the index of Slater determinants in full space, variational space and the space connected to $\mathcal{V}^{(l)}$ but not in $\mathcal{V}^{(l)}$, respectively, which satisfy

$$\begin{aligned}\mathcal{N}^{(l)} &= \text{supp}(\boldsymbol{b}^{(l)})\\ \mathcal{V}^{(l)} &= \text{supp}(\boldsymbol{c}^{(l)})\\ \mathcal{P}^{(l)} &= \text{supp}(\boldsymbol{b}^{(l)})/\text{supp}(\boldsymbol{c}^{(l)})\end{aligned} \tag{6}$$

https://doi.org/10.1021/acs.jctc.6c00103
J. Chem. Theory Comput. 2026, 22, 5005−5019

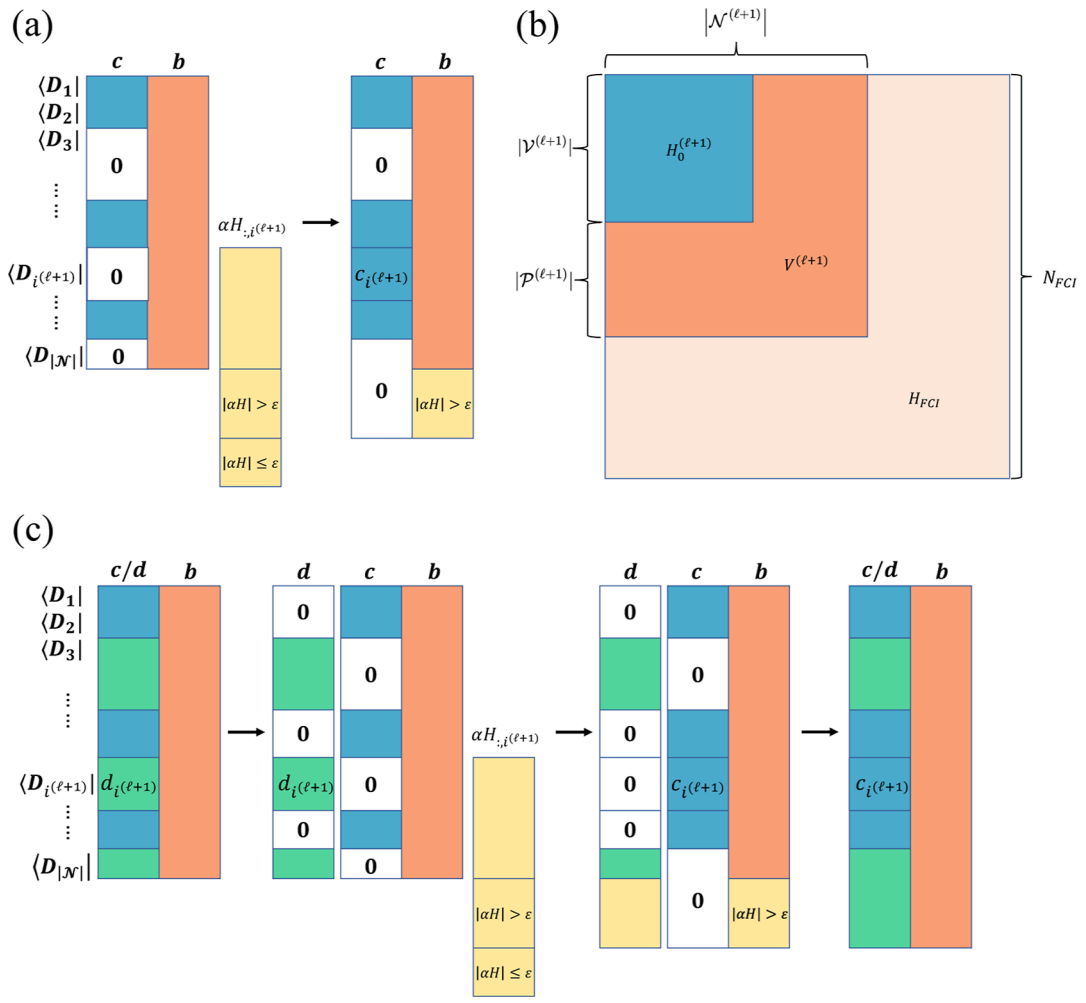

Figure 2. Schematic representations of the coefficient-update of CDFCI and IP-CDFCI algorithms and the partition of FCI Hamiltonian. (a) This figure represents the updates of $\boldsymbol{c}$ and the compressed update of $\boldsymbol{b}$ in the CDFCI algorithm, where the yellow region corresponds to the nonzero elements of $\mathcal{I}_H(i^{(l+1)})$. (b) This figure illustrates the partitioning of the entire FCI Hamiltonian matrix. From largest to smallest, there is the full FCI Hamiltonian matrix of dimension N_{FCI}, the perturbative Hamiltonian matrix of dimension $|\mathcal{N}^{(l+1)}|$, and the variational Hamiltonian matrix of dimension $|\mathcal{V}^{(l+1)}|$. Without loss of generality, we group the indices belonging to different spaces together and represent them in the form of submatrices. (c) This figure shows the updates of $\boldsymbol{c}$, $\boldsymbol{b}$, and $\boldsymbol{d}$ in the IP-CDFCI algorithm. During the update process, the stored $\boldsymbol{c}$ and $\boldsymbol{d}$ are separated and calculated and updated using different formulas, while the orthogonal relationship between $\boldsymbol{c}$ and $\boldsymbol{d}$ is always maintained.

In the code implementation, CDFCI uses a hash table constructed based on the mapping between a binary string and the coefficients of the vectors to store the computed $\boldsymbol{c}$ and $\boldsymbol{b}$ during the calculation process, as shown in the Figure 1a. For a determinant belonging to $\mathcal{V}$, it must also belong to $\mathcal{N}$. However, a determinant belonging to $\mathcal{N}$ does not necessarily belong to $\mathcal{V}$. Therefore, the vector $\boldsymbol{c}$, which is stored together with $\boldsymbol{b}$, contains many zero elements.

2.1. Determinant-Select and Coefficient-Update Scheme

Assuming we have coefficient vectors $\boldsymbol{c}^{(l)}$ and $\boldsymbol{b}^{(l)}$ in the l-th iteration, we update them to $\boldsymbol{c}^{(l+1)}$ and $\boldsymbol{b}^{(l+1)_{+1}}$, respectively. We use an approximate gradient to select the determinant to update

$$i^{(l+1)} = \underset{j\in\mathcal{I}_H(i^{(l)})}{\mathrm{argmax}} |\nabla_j f(\boldsymbol{c}^{(l)})| \tag{7}$$

We then update $\boldsymbol{c}^{(l)}$ according to a line search step size α

$$c_j^{(l+1)} = \begin{cases} c_j^{(l)} + \underset{\tilde{\alpha}}{\arg\min} f(\boldsymbol{c}^{(l)} + \boldsymbol{e}_j\tilde{\alpha}), j = i^{(l+1)} \\ c_j^{(l)}, j \neq i^{(l+1)} \end{cases} \tag{8}$$

If $i^{(l+1)} \notin \mathcal{V}^{(l)}$, the variational space $\mathcal{V}^{(l+1)}$ will be expanded by one new determinant, causing $\mathcal{P}^{(l+1)}$ to shrink. We can update $\boldsymbol{b}^{(l+1)}$ with compression based on the updated $\boldsymbol{c}^{(l+1)}$

$$b_j^{(l+1)} = \begin{cases} b_j^{(l)} + \alpha H_{j,i^{(l+1)}}, j \in \mathcal{N}^{(l)} \\ \alpha H_{j,i^{(l+1)}}, \quad |\alpha H_{j,i^{(l+1)}}| > \varepsilon \\ 0, \quad \text{otherwise} \end{cases} \tag{9}$$

where $j \in \mathcal{I}_H(i^{(l+1)})$ because our update scheme is conducted in the H-connected space of $|D_{i^{(l+1)}}\rangle$.

The updating of $b_j^{(l+1)}$ for $j \notin \mathcal{N}^{(l)}$ will expand $\mathcal{N}^{(l+1)}$ and $\mathcal{P}^{(l+1)}$ while $\mathcal{V}^{(l+1)}$ will remain unchanged. We will recalculate

https://doi.org/10.1021/acs.jctc.6c00103
J. Chem. Theory Comput. 2026, 22, 5005−5019

$b_{i^{(l+1)}}^{(l+1)}$ exactly, which ensures the exact estimated variational energy. A schematic representation of the coefficient-update of CDFCI algorithm is shown in Figure 2a.

2.2. Variational Energy

Although CDFCI uses compression techniques, the variational energy, i.e., Rayleigh quotient $r(\boldsymbol{c}) = \frac{\boldsymbol{c}^{\mathrm{T}}H\boldsymbol{c}}{\boldsymbol{c}^{\mathrm{T}}\boldsymbol{c}}$, is of second order accuracy for $\boldsymbol{c}^{(l+1)}$. The variational energy in each iteration is given by[31]

$$E_0^{(l+1)} = \frac{(\boldsymbol{c}^{(l+1)})^{\mathrm{T}}H\boldsymbol{c}^{(l+1)}}{(\boldsymbol{c}^{(l+1)})^{\mathrm{T}}\boldsymbol{c}^{(l+1)}} \tag{10}$$

In terms of CDFCI iterative feature, we do not need to calculate variational energy explicitly in each iteration. According to coefficient update strategy, the updating of denominator needs the information on line search step size and coefficient $c_{i^{(l+1)}}^{(l)}$

$$(\boldsymbol{c}^{(l+1)})^{\mathrm{T}}\boldsymbol{c}^{(l+1)} = (\boldsymbol{c}^{(l)})^{\mathrm{T}}\boldsymbol{c}^{(l)} + 2\alpha c_{i^{(l+1)}}^{(l)} + \alpha^2 \tag{11}$$

and the numerator is updated by coefficient $b_{i^{(l+1)}}^{(l+1)}$ and diagonal element $H_{i^{(l+1)},i^{(l+1)}}$

$$(\boldsymbol{c}^{(l+1)})^{\mathrm{T}}H\boldsymbol{c}^{(l+1)} = (\boldsymbol{c}^{(l)})^{\mathrm{T}}H\boldsymbol{c}^{(l)} + 2\alpha b_{i^{(l+1)}}^{(l+1)} - \alpha^2 H_{i^{(l+1)},i^{(l+1)}} \tag{12}$$

The only approximate term $b_{i^{(l+1)}}^{(l+1)}$ is recalculated exactly, and the variational energy is calculated by a constantly increasing variational space $\mathcal{V}^{(l)}$ within $|\mathcal{N}^{(l)}|$. We can update variational energy $E_0^{(l+1)}$ along with the updating $\boldsymbol{c}^{(l+1)}$ and $\boldsymbol{b}^{(l+1)}$ in each iteration without any extra computing resource or memory. This formula is much more accurate than the mixed estimator commonly used in FCIQMC, where the latter is of first order accuracy.

2.3. Perturbative Coordinate-Descent FCI

For the second quantization Hamiltonian matrix in the Fock space, its dimension is 2^M, where M is the number of basis sets in the single-particle Hilbert space. The FCI problem deals with a subspace within this large Fock space, which restricts the total number of particles for Slater determinant configurations to be N, alone with the spin multiplicity and molecular point group restriction, as shown in eq 2. Therefore, the dimension of the Hamiltonian matrix for the FCI problem is N_{FCI}, where $N_{\mathrm{FCI}} = O\left(\left(\frac{M/2}{N/2}\right)^2\right) \ll 2^M$. However, N_{FCI} is still too large for practical purposes. The CDFCI or SCI algorithm aims to find a submatrix of the FCI Hamiltonian matrix by solving for the smallest eigenvalue of this expanding submatrix, approximating the smallest eigenvalue of the full FCI Hamiltonian matrix. Different SCI algorithms correspond to different schemes for enlarging the submatrix dimension, or in other words, selecting criteria for new Slater determinants. In the context of CDFCI algorithm, the indices of this submatrix coefficients belong to $\mathcal{V}$, and we aim to obtain the smallest eigenvalue of this submatrix with the smallest possible $|\mathcal{V}|$ in order to approximate the true ground state energy. The dimension of the submatrix increases with each iteration step, corresponding to the expansion of the variational space, as shown in eq 8. We can write the eigenvalue equation of the submatrix of total FCI Hamiltonian matrix

$$H_0^{(l+1)}\tilde{\boldsymbol{c}}^{(l+1)} = E_0^{(l+1)}\tilde{\boldsymbol{c}}^{(l+1)} \tag{13}$$

where the eigenvector $\tilde{\boldsymbol{c}}^{(l+1)}$ and eigenvalue $E_0^{(l+1)}$ are different from $\boldsymbol{c}^{(l+1)}$ and Rayleigh quotient $r(\boldsymbol{c}^{(l+1)})$ unless CDFCI has been converged at $(l+1)$-th iteration. In practical calculations they are good approximation to exact eigenpair, we approximate the exact zero-th order eigenvalue and eigenvector by Rayleigh quotient and wave function coefficient vector computed in the l-th iteration of CDFCI. In the actual CDFCI algorithm, in order to obtain gradient information and compute the Rayleigh quotient, we also need to simultaneously deal with a sparse vector $\boldsymbol{b}$. In $l+1$-th iteration, we always have $\mathcal{V}^{(l+1)} \subseteq \mathcal{N}^{(l+1)}$,

The space of $\mathcal{N}^{(l+1)}$ can be divided into a variational part $\mathcal{V}^{(l+1)}$ and a perturbative part $\mathcal{P}^{(l+1)}$. According to this partition, we also divide the selected Hamiltonian submatrix into two parts based on $\mathcal{V}^{(l+1)}$ and $\mathcal{P}^{(l+1)}$ as follows

$$\begin{aligned} H^{(l+1)} &= \sum_{m,n\in\mathcal{N}^{(l+1)}} H_{m,n}|D_m\rangle\langle D_n| \\ &= H_0^{(l+1)} + V^{(l+1)} \end{aligned} \tag{14}$$

where

$$H_0^{(l+1)} = \sum_{i,j\in\mathcal{V}^{(l+1)}} H_{i,j}|D_i\rangle\langle D_j| + \sum_{a\in\mathcal{P}^{(l+1)}} H_{a,a}|D_a\rangle\langle D_a| \tag{15}$$

and

$$V^{(l+1)} = H^{(l+1)} - H_0^{(l+1)} \tag{16}$$

A schematic representation of the partition of FCI Hamiltonian is shown in Figure 2b. It is worth noting the key distinction between the PT framework adopted herein and the standard SCI + PT (e.g., EN-PT2 in SHCI) approaches. In standard SCI + PT, researchers first select a critical configuration subspace $\mathcal{N}$ (whose dimension is much smaller than the full FCI dimension N_{FCI}) via specific criteria, compute the ground-state eigenvector and energy within this subspace, and subsequently apply second-order perturbation corrections over the entire Hilbert space corresponding to N_{FCI} outside $\mathcal{N}$—a process that often requires stochastic schemes due to the enormous dimension N_{FCI}. In contrast, our PT framework (for both CDFCI + PT and IP-CDFCI) restricts the perturbation correction within $\mathcal{N}$ (the compressed subspace selected via parameter ϵ) rather than the full space of dimension N_{FCI}. Specifically, during the CDFCI iteration, as the wave function $\boldsymbol{c}$ gradually expands toward $\mathcal{N}$ but remains smaller than $\mathcal{N}$, we use the variational energy derived from the iterative $\boldsymbol{c}$ (not the eigenenergy of the fully converged $\mathcal{N}$) as the zero-order energy, and perform perturbation corrections within $\mathcal{N}$ outside the current dimension of $\boldsymbol{c}$. This distinction explains why our benchmarks compare with the variational energies of HCI and DMRG (rather than their PT-augmented versions), as our perturbation is confined to the subspace typically regarded as the variational space in standard SCI.

As previously mentioned, the dimension of the variational space and the total $\mathcal{N}^{(l+1)}$ will increase along with the CDFCI iteration. CDFCI selects/visits determinants based on their importance, so it captures the most important physical information in the variational space. In principle the converged variational wave function and ground state energy contribute dynamic and static correlation simultaneously, however in

https://doi.org/10.1021/acs.jctc.6c00103
J. Chem. Theory Comput. 2026, 22, 5005−5019

practical calculation people usually cut off the iteration when it converges to a relative rough threshold and hence $\mathcal{V}^{(l+1)} \neq \mathcal{N}^{(l+1)}$ or $\mathcal{P}^{(l+1)} \neq \emptyset$. At such practical situation, the variational space $\mathcal{V}^{(l+1)}$ captures dominant static correlation and strong dynamic correlation, while the perturbative space $\mathcal{P}^{(l+1)}$ captures weak residual dynamic correlation not yet absorbed by $\mathcal{V}^{(l+1)}$. The two spaces are not strictly segregated—static correlation is primarily handled by $\mathcal{V}^{(l+1)}$, but dynamic correlation is distributed across both spaces, especially for strongly correlated systems. Neglecting this part of dynamic correlation can lead to quantitatively incorrect results. Therefore, it is reasonable to treat the determinants outside the variational space in a perturbative way, considering the trade-off between accuracy and computing time.

According to eqs 14−16 and perturbation theory, we approximate the zero-th order wave function coefficients as $c_i^{(l+1)}$ and according to which derive the expression of first order wave function in l + 1-th iteration[32]

$$\left|\Psi_0^{(l+1)}\right\rangle = \sum_{i\in\mathcal{V}^{(l+1)}} c_i^{(l+1)}|D_i\rangle$$

$$\left|\Psi_1^{(l+1)}\right\rangle = \sum_{a\in\mathcal{P}^{(l+1)}} \frac{\sum_{i\in\mathcal{V}^{(l+1)}} H_{a,i}c_i}{E_0^{(l)} - H_{a,a}}|D_a\rangle \tag{17}$$

The second-order perturbative energy in l + 1-th iteration is given by

$$\Delta E_2^{(l+1)} = \langle\Psi_0^{(l+1)}|V^{(l+1)}|\Psi_1^{(l+1)}\rangle$$

$$= \sum_{a\in\mathcal{P}^{(l+1)}} \frac{\left(\sum_{i\in\mathcal{V}^{(l+1)}} H_{a,i}c_i\right)^2}{E_0^{(l)} - H_{a,a}} \tag{18}$$

Exact formula is difficult to evaluate directly, but we notice that CDFCI already calculates and stores a compressed vector $\boldsymbol{b}^{(l+1)}$

$$b_a^{(l+1)} \approx \sum_{i\in\mathcal{V}^{(l+1)}} H_{a,i}c_i^{(l+1)} \tag{19}$$

which could replace the sum in the numerator to avoid redundant computation and memory cost. Hence, we can write the perturbative wave function and second-order perturbative energy as

$$|\Psi_1^{(l+1)}\rangle \approx \sum_{a\in\mathcal{P}^{(l+1)}} \frac{b_a^{(l+1)}}{E_0^{(l)} - H_{a,a}}|D_a\rangle \tag{20}$$

and

$$\Delta E_2^{(l+1)} \approx \sum_{a\in\mathcal{P}^{(l+1)}} \frac{(b_a^{(l+1)})^2}{E_0^{(l)} - H_{a,a}}$$

$$= \sum_{a\in\mathcal{P}^{(l+1)}} b_a^{(l+1)} d_a^{(l+1)} \tag{21}$$

where $\boldsymbol{d}^{(l+1)}$ is the coefficient vector of the approximated first order perturbative wave function

$$d_a^{(l+1)} = \frac{b_a^{(l+1)}}{E_0^{(l)} - H_{a,a}} \tag{22}$$

If we set the compression parameter to 0, the sparse vector $\boldsymbol{b}$ is exactly equal to $H\boldsymbol{c}$. In this case, the exact perturbative wave function can be calculated using $\boldsymbol{b}$ without any approximation.

Here, we present two approaches for computing perturbation energy.

The first approach is similar to standard SCI + PT or HCI + PT methods, where the entire computation is divided into two stages: the variational stage and the perturbative stage. These two stages are treated as independent modules that do not interfere with each other. The calculation of perturbation energy is performed as a postprocessing step after the variational stage, using the variational wave function and the variational ground state energy obtained from the variational stage. The required perturbation energy is then computed by summing over the entire $\mathcal{P}$. We denote this approach as coordinate descent full configuration interaction plus perturbation theory (CDFCI + PT).

The second approach involves embedding the computation of perturbative wave function and energy within the variational stage, based on the iterative nature of the CDFCI algorithm. The advantage of this approach is that during the variational stage, we can capture the current static and dynamic correlations in each iteration. Additionally, we can estimate the error magnitude with respect to the true FCI ground state energy by updating the magnitude of the perturbation energy at each iteration step. However, this iterative perturbation scheme introduces small errors compared to the exact perturbation formula. We denote this approach as iterative perturbative coordinate descent full configuration interaction (IP-CDFCI).

For the first approach CDFCI + PT, we aim to perform a sufficiently iterative variational process to obtain a reliable variational wave function and energy. Then, we perform a single calculation of the perturbation energy to further refine the variational energy.

In the second approach IP-CDFCI, we intend to compute the perturbation energy at each iteration of the variational calculation in CDFCI (which typically involves tens of thousands to billions of iterations). Essentially, each individual iteration of CDFCI incorporates both the variational and perturbative stages. We expect to obtain a perturbation energy convergence curve similar to the variational energy convergence curve. However, if we simply include the perturbative stage within each CDFCI iteration, the computational cost would become unmanageable.

2.4. Coordinate-Descent FCI plus Perturbation Theory

The CDFCI + PT method is similar to traditional SCI + PT or HCI + PT methods, the calculation of perturbation energy is performed as a postprocessing step after the variational stage, using the variational wave function and the variational ground state energy obtained from the variational stage, which corresponds to the standard CDFCI algorithm. In the perturbation stage, these results are used in eq 18 to calculate the second-order perturbative correction, further capturing the dynamic correlation effects lost in the variational process. Similarly, we can use the compressed sparse vector $\boldsymbol{b} \approx H\boldsymbol{c}$ to replace the summation in the numerator, and use eq 21 to calculate a compressed perturbative correction. This way, the computational cost in the entire perturbation stage is reduced to a single traversal summation calculation in the $\mathcal{P}$ space. As shown in Figure 1a, CDFCI continuously stores the sparse vectors $\boldsymbol{c}$ and $\boldsymbol{b}$, so there is no need for additional memory space in the perturbation stage. Or we can also use eq 18 by

https://doi.org/10.1021/acs.jctc.6c00103
J. Chem. Theory Comput. 2026, 22, 5005−5019

reevaluating numerator Hc to calculate an exact perturbative energy, where the perturbation Hamiltonian is defined by Figure 2b.

The advantage of CDFCI + PT is that it can obtain an exact perturbative energy without approximation (when the compression parameter ε is set to 0), and it requires less computational effort compared to IP-CDFCI with the same number of variational iterations. However, the drawback of CDFCI + PT is that it can only obtain the final perturbative energy correction. It cannot provide an estimate of the perturbative energy in the early stages of the variational stage, like IP-CDFCI, nor can it obtain system correlation information from the perturbative energy iterations.

The pseudocode for CDFCI + PT is simply implementing eq 21 once with the sparse vector $\boldsymbol{b}$ after the variational iteration loop of the standard CDFCI algorithm, which presented in Algorithm 1 along with variational CDFCI.

Algorithm 1: Coordinate-descent FCI plus perturbation theory

Data: FCIDUMP

Result: Variational energy E_0 and perturbative energy ΔE_2

Initialization;

$i^{(0)} = |D_{\text{ref}}\rangle, \boldsymbol{c}^{(0)} = \boldsymbol{e}_{\text{ref}}, \boldsymbol{b}^{(0)} = \boldsymbol{0}, \varepsilon$;

for $\ell = 0, 1, 2, \ldots$ **do**

  Select determinant $|D_{i^{(\ell+1)}}\rangle$ by Eq. 7;

  Solve $\alpha = \underset{\tilde{\alpha}\in\mathbb{R}}{\operatorname{argmin}} f\left(\boldsymbol{c}^{(\ell)} + \tilde{\alpha}\boldsymbol{e}_{i^{(\ell+1)}}\right)$;

  Update variational wave function $\boldsymbol{c}^{(\ell+1)}$ by Eq. 8;

  Update $\left(\boldsymbol{c}^{(\ell+1)}\right)^{\top}\boldsymbol{c}^{(\ell+1)}$ by Eq. 11;

  for $j \in \mathcal{I}_H(i^{(\ell+1)})$ **do**

    Update perturbative coefficients $b_j^{(\ell+1)}$ by Eq. 9

    Recalculate $b_{i^{(\ell+1)}}^{(\ell+1)} = \sum_j H_{i^{(\ell+1)},j} c_j^{(\ell+1)}$

  end

  Update $\left(\boldsymbol{c}^{(\ell+1)}\right)^{\top} H\boldsymbol{c}^{(\ell+1)}$ by Eq. 12;

  Update $E_0^{(\ell+1)}$ by Eq. 10;

  if *converge* **then**

    Break;

  end

end

Evaluate ΔE_2 by Eq. 21.

2.5. Iterative Perturbative Coordinate-Descent FCI

The direct implementation of iterative perturbation energy is to embed a perturbative stage into each CDFCI variational iteration, but after a long time iteration, the dimension of space of $\mathcal{N}^{(I+1)}$ will be extremely large, at this time, the summation over total perturbative space $\mathcal{P}^{(I+1)}$ in each iteration is unacceptable in FCI problem.

The original CDFCI only works on the space of $\mathcal{I}_H(i^{(I)})$ which is much smaller than the space of $\mathcal{N}^{(I)}$. In order to make the perturbation calculation more consistent with original CDFCI, here we propose an approximate iterative scheme to calculate the perturbative wave function and energy efficiently in each iteration.

To update $\boldsymbol{d}$ along with $\boldsymbol{c}$ and $\boldsymbol{b}$, we propose an iterative scheme that avoids the expensive summation over total $\mathcal{P}^{(I)}$ but only focus on $\mathcal{I}_H(i^{(I+1)})$ in each iteration. Specifically, the iterative update of $\boldsymbol{d}$ is given by

$$\Delta d_a^{(I+1)} = d_a^{(I+1)} - d_a^{(I)} \tag{23}$$

Using this update scheme for $\boldsymbol{d}^{(I+1)}$, we can also iteratively update the perturbative energy according to

$$\Delta E_2^{(I+1)} = \Delta E_2^{(I)} + \sum_{a\in\mathcal{P}^{(I+1)}} b_a^{(I+1)} \Delta d_a^{(I+1)} \tag{24}$$

We arise a coefficient update scheme for $\boldsymbol{d}$ to calculate perturbative correction along with updating $\boldsymbol{c}^{(I+1)}$ and $\boldsymbol{b}^{(I+1)}$ in CDFCI.

2.5.1. Update $\boldsymbol{c}^{(I+1)}$. In $I+1$-iteration, we update $\boldsymbol{c}^{(I+1)}$ only by one determinant $|D_{i^{(I+1)}}\rangle$. $\boldsymbol{i}^{(I+1)}$ represents the index of the determinant to be added to $\mathcal{V}^{(I)}$. There are two cases here. (i) If $i^{(I+1)} \in \mathcal{V}^{(I)}$), after updating $\boldsymbol{c}^{(I+1)}$, $|\mathcal{V}^{(I+1)}| = |\mathcal{V}^{(I)}|$, $|\mathcal{P}^{(I+1)}| = |\mathcal{P}^{(I)}|$, and $\boldsymbol{d}^{(I+1)}$ does not need to be updated. (ii) If $i^{(I+1)} \notin \mathcal{V}^{(I)}$, after updating $\boldsymbol{c}^{(I+1)}$, $|\mathcal{V}^{(I+1)}| = |\mathcal{V}^{(I)}| + 1$, $|\mathcal{P}^{(I+1)}| = |\mathcal{P}^{(I)}| - 1$, and we update $\boldsymbol{d}^{(I+1)}$ according to

$$d_a^{(I+1)} = \begin{cases} 0, & a = i^{(I+1)} \notin \mathcal{V}^{(I)} \\ d_a^{(I)}, & \text{otherwise.} \end{cases} \tag{25}$$

2.5.2. Update $\boldsymbol{b}^{(I+1)}$. In $I+1$-iteration, we update $b_j^{(I+1)} = b_j^{(I)} + \alpha H_{j,i^{(I+1)}}$ in three cases. (i) The first case is when the determinant $|D_j\rangle$ is already selected in $\mathcal{V}^{(I)}$, which means that neither $\mathcal{V}^{(I+1)}$ nor $\mathcal{N}^{(I+1)}$ changes in dimension, $|\mathcal{V}^{(I+1)}| = |\mathcal{V}^{(I)}|, |\mathcal{P}^{(I+1)}| = |\mathcal{P}^{(I)}|$, and we do not need to update $\boldsymbol{d}^{(I+1)}$. (ii) In the second case, the determinant $|D_j\rangle$ is already selected in $\mathcal{N}^{(I)}$ but not in $\mathcal{V}^{(I)}$, which means we need to recalculate $d_j^{(I+1)}$ using the newly updated $b_j^{(I+1)}$ and the variational energy from the last iteration

$$d_j^{(I+1)} = \frac{b_j^{(I+1)}}{E_0^{(I)} - H_{j,j}} \tag{26}$$

here we maintain $|\mathcal{V}^{(I+1)}| = |\mathcal{V}^{(I)}|, |\mathcal{P}^{(I+1)}| = |\mathcal{P}^{(I)}|$. (iii) In the third case, the determinant $|D_j\rangle$ is a new determinant not in $\mathcal{N}^{(I)}$ or $\mathcal{V}^{(I)}$. We update $b_j^{(I+1)} = \alpha H_{j,i^{(I+1)}}$ only if $|\alpha H_{j,i^{(I+1)}}| > \varepsilon$. This update adds a new determinant to $\mathcal{N}^{(I+1)}$ and $\mathcal{P}^{(I+1)}$. Hence, we update $d_j^{(I+1)}$ as

$$d_j^{(I+1)} = \frac{\alpha H_{j,i^{(I+1)}}}{E_0^{(I)} - H_{j,j}} \tag{27}$$

In such case, we have $|\mathcal{V}^{(I+1)}| = |\mathcal{V}^{(I)}|$ and $|\mathcal{P}^{(I+1)}| = |\mathcal{P}^{(I)}| + 1$. In other cases, we do not update $\boldsymbol{b}^{(I+1)}$ or $\boldsymbol{d}^{(I+1)}$. We summarize the update scheme for $\boldsymbol{d}^{(I+1)}$ as follows

$$d_j^{(I+1)} = \begin{cases} \dfrac{b_j^{(I+1)}}{E_0^{(I)} - H_{j,j}}, & j \in \mathcal{P}^{(I)} \\ \dfrac{\alpha H_{j,i^{(I+1)}}}{E_0^{(I)} - H_{j,j}}, & \left|\alpha H_{j,i}^{(I+1)}\right| > \varepsilon \\ 0, & \text{otherwise} \end{cases} \tag{28}$$

where $j \in \mathcal{I}_H(i^{(I+1)})$ because our update scheme is conducted in the H-connected space of $|D_{i^{(I+1)}}\rangle$. It is important to note that the update rule for d differs from that of $\boldsymbol{b}^{(I+1)}$, owing to the distinct

https://doi.org/10.1021/acs.jctc.6c00103
J. Chem. Theory Comput. 2026, 22, 5005−5019

spaces they occupy: the combined dimension of $\boldsymbol{d}^{(l+1)}$ and $\boldsymbol{c}^{(l+1)}$ is equivalent to the dimension of $\boldsymbol{b}^{(l+1)}$, meaning $\boldsymbol{d}^{(l+1)}$ and $\boldsymbol{c}^{(l+1)}$ together occupy a space of the same size as $\boldsymbol{b}^{(l+1)}$. A schematic representation of the coefficient-update of IP-CDFCI algorithm is shown in Figure 2c. The figure includes four processes. In the actual program implementation, the transition/update from the first state to the last state is direct. The two intermediate processes in the middle serve only an illustrative purpose and do not represent the actual computational steps.

Our iterative update strategy of $\boldsymbol{d}^{(l+1)}$ release the expensive sum over total $\mathcal{P}^{(l+1)}$, but it introduce an intrinsic difference between our $d_a^{(l+1)}$ and the exact $\frac{b_a^{(l+1)}}{E_0^{(l)} - H_{a,a}}$ at a certain iteration l. This is because there may be a determinant $|D_k\rangle$ in $\boldsymbol{d}$ that is only updated a few times at the early iterations. After a long iteration, d_k still only remembers the perturbation calculated by the earlier variational energy, $d_k^{(l)} = \frac{b_k^{(l)}}{E_0^{(n)} - H_{a,a}}$, where n is the last iteration that d_k was updated. However, numerical results demonstrate that such errors are small and can be ignored. We believe there are two reasons for this. First, the variational energy converges relatively smoothly in CDFCI, and the small difference in the denominator will be further reduced. Second, due to the nice feature of CDFCI which always catches the appreciative determinants, for important perturbative d_k which carries a large b_k, the Rayleigh quotient in denominator will be updated more frequently, which also reduces the error.

We conclude this section with a pseudocode for IP-CDFCI shown in Algorithm 2.

Algorithm 2: Iterative perturbative coordinate-descent FCI

Data: FCIDUMP

Result: Variational energy E_0 and Perturbative energy ΔE_2

Initialization;

$i^{(0)} = |D_{\text{ref}}\rangle, \boldsymbol{c}^{(0)} = \boldsymbol{e}_{\text{ref}}, \boldsymbol{b}^{(0)} = \boldsymbol{0}, E_0^{(0)} = E_{\text{ref}}, \varepsilon$;

for $\ell = 0, 1, 2, \ldots$ **do**

- Select determinant $|D_{i^{(\ell+1)}}\rangle$ by Eq. 7;
- Solve $\alpha = \underset{\alpha \in \mathbb{R}}{\text{argmin}} f\left(\boldsymbol{c}^{(\ell)} + \alpha \boldsymbol{e}_{i^{(\ell+1)}}\right)$;
- Update $\boldsymbol{c}^{(\ell+1)}$ by Eq. 8;
- Update $\boldsymbol{d}^{(\ell+1)}$ if $i^{(\ell+1)} \notin \text{supp}\left(\boldsymbol{c}^{(\ell)}\right)$ by Eq. 25;
- Update $\left(\boldsymbol{c}^{(\ell+1)}\right)^\top \boldsymbol{c}^{(\ell+1)}$ by Eq. 11;
- **for** $j \in \mathcal{I}_H(i^{(\ell+1)})$ **do**
  - Update $b_j^{(\ell+1)}$ by Eq. 9;
  - Update $d_j^{(\ell+1)}$ by Eq. 28;
  - Recalculate $b_{i^{(\ell+1)}}^{(\ell+1)} = \sum_j H_{i^{(\ell+1)},j} c_j^{(\ell+1)}$;
- **end**
- Update $\left(\boldsymbol{c}^{(\ell+1)}\right)^\top H \boldsymbol{c}^{(\ell+1)}$ by Eq. 12;
- Update $E_0^{(\ell+1)}$ by Eq. 10;
- Update $\Delta E_2^{(\ell+1)}$ by Eq. 24;
- **if** *converge* **then**
  - Break;
- **end**

end

3. IMPLEMENTATION

We now give some implementation details of algorithm, focusing on the IP-CDFCI algorithm while the CDFCI + PT is only a postprocessing of standard CDFCI.

The original CDFCI formula stores two sparse vectors $\boldsymbol{c}$ and $\boldsymbol{b}$ in memory simultaneously as shown in Figure 1a and they are updated as shown in Figure 2a. However, the entries of $\boldsymbol{c}$ in $\mathcal{P}^{(l)}$ are all zeros stored in real hash table, which wastes memory. To optimize the formula, we propose using the entries of $\boldsymbol{c}$ in $\mathcal{P}^{(l)}$ to store the coefficient vector $\boldsymbol{d}^{(l+1)}$ of the perturbative wave function due to the orthogonality relation between variational and perturbative wave function. This way, we can calculate the perturbative energy using the stored values of $\boldsymbol{d}^{(l+1)}$ based on our approximate perturbative formula. Additionally, the supports of sparse vectors $\boldsymbol{c}^{(l)}$ and $\boldsymbol{d}^{(l)}$ should be disjoint, and their union should be equal to the support of $\boldsymbol{b}^{(l+1)}$

$$\begin{aligned} &\text{supp}(\boldsymbol{d}^{(l)}) = \mathcal{P}^{(l)} \\ &\text{supp}(\boldsymbol{c}^{(l)}) \cup \text{supp}(\boldsymbol{d}^{(l)}) = \mathcal{N}^{(l)} \\ &\text{supp}(\boldsymbol{c}^{(l)}) \cap \text{supp}(\boldsymbol{d}^{(l)}) = \emptyset \end{aligned} \tag{29}$$

To optimize the memory structure of CDFCI with perturbative correction, we store $\boldsymbol{c}$ and $\boldsymbol{d}$ in the same vector while retaining the memory structure of the original CDFCI, thus avoiding any extra memory cost, as shown in the Figure 1b. This allows us to calculate the perturbative energy without incurring any additional memory costs compared to the original CDFCI, as shown in the Figure 2c.

In IP-CDFCI, we store three sparse vectors $\boldsymbol{c}$, $\boldsymbol{b}$, and $\boldsymbol{d}$ in a hash table with the same size as in original CDFCI. This still looks like two column vectors, one for $\boldsymbol{b}$ and another for the mix of $\boldsymbol{c}$ and $\boldsymbol{d}$, which can be interpreted as $|\Psi_0\rangle + |\Psi_1\rangle$. In CDFCI, the indices of Slater determinants are encoded in an n_{orb}-bit binary string, with each bit representing the occupation of a spin−orbital.

We store $\boldsymbol{c}$ and $\boldsymbol{d}$ in a mixed way, but we cannot distinguish an entry belonging to $\boldsymbol{c}$ or $\boldsymbol{d}$ when conducting coefficient updating of $\boldsymbol{b}$, $\boldsymbol{c}$, and $\boldsymbol{d}$ in IP-CDFCI for the different update schemes of $\boldsymbol{c}$ and $\boldsymbol{d}$.

So in IP-CDFCI, we use a $(n_{\text{orb}} + 1)$-bit binary string to represent the indices of Slater determinants. For determinants in the Hash table, we use the highest bit to identify the ownership of the determinant, which we call the "perturb bit". If the perturb bit equals 1, it means the determinant is in the variational space $\mathcal{V}$ and belongs to $\boldsymbol{c}$. If it equals 0, the determinant is in the perturbative space $\mathcal{P}$ and belongs to $\boldsymbol{d}$. If the $(n_{\text{orb}} + 1)$-bit binary string is stored as an array of 64 bit integers, $\left\lceil \frac{n_{\text{orb}} + 1}{64} \right\rceil$ integers are needed to represent the index of a determinant. A schematic representation of hash table and perturb bit is shown in Figure 1b.

When updating $\boldsymbol{b}^{(l+1)}$, we need to evaluate all the Hamiltonian matrix elements connected to $|D_{i^{(l+1)}}\rangle$ and one-by-one check whether the determinant is an "old" determinant already selected in the Hash table. Such data access procedure can be the most expensive part during the whole calculation. We need to identify the ownership of the determinant by the perturb bit. Using the original hash function, we need to find the determinant twice in the hash table for perturb bit equal to 0 and 1, respectively. This would almost double the computational time and is unacceptable. However, considering that the "perturb bit" at the highest bit position of the last integer does not indicate a real occupation of a spin−orbital, we can modify the hash function to ignore the perturb bit and only map the "effective" configuration string to an array index, which only involves several efficient bit operations. Therefore, IP-CDFCI

https://doi.org/10.1021/acs.jctc.6c00103
J. Chem. Theory Comput. 2026, 22, 5005−5019

still only searches for a determinant in the Hash table once, and if it is found, then we check the perturb bit to identify its belonging.

Besides the ownership problem of determinants in the hash table, the perturbative calculation introduces extra computation for evaluating the vector $\boldsymbol{d}$. The coefficients of $\boldsymbol{d}$ are updated along with the variational energy and the update of $\boldsymbol{b}$. The computational expensive part is the evaluation of the diagonal element $H_{a,a}$, which is required for updating the coefficient d_a. In original CDFCI, the most computationally expensive part is the evaluation of $H_{:,i^{(l+1)}}$ except for the data accessing step, which requires evaluating $O(N_H)$ entries of the Hamiltonian matrix when updating $\boldsymbol{b}$, where $N_H = \max_i|\mathcal{I}_H(i)|$ is the maximum number of nonzero entries in columns of Hamiltonian matrix. For perturbative calculation, it also requires evaluating $O(N_H)$ diagonal entries of Hamiltonian to update $\boldsymbol{d}$. The total computational time with the expensive evaluation of diagonal entries of Hamiltonian and calculation of $\boldsymbol{d}$ is almost three times than original CDFCI after certain iterations [24h/8h, Cr_2]. Nonetheless, considering both variational energy and perturbative energy, IP-CDFCI is still more economical than the original approach with a much faster convergence speed and a much lower energy up to a certain computing time.

We have also devised a strategy to eliminate the costly repetitive evaluation of diagonal elements of the Hamiltonian, which trades memory usage for computational time savings. In the original CDFCI, $\boldsymbol{c}$ and $\boldsymbol{b}$ are stored together with some redundant memory used for some zero entries of $\boldsymbol{c}$. In IP-CDFCI, $\boldsymbol{c}$, $\boldsymbol{b}$, and $\boldsymbol{d}$ are stored together, and the redundant vector entries of $\boldsymbol{c}$ are used to store $\boldsymbol{d}$, which requires repeatedly evaluating $H_{a,a}$. To solve this issue, we create a third vector, $\boldsymbol{h}$, which has the same length as $\boldsymbol{b}$ and stores the diagonal entries of the Hamiltonian, with $\mathrm{supp}(\boldsymbol{h}) = \mathrm{supp}(\boldsymbol{b})$. We initialize $\boldsymbol{h}$ as the energy of the reference state and fill up the entries during the updating of $\boldsymbol{b}$. Therefore, we can reuse $H_{a,a}$ when updating $\boldsymbol{d}$, as $\mathrm{supp}(\boldsymbol{d}) \subset \mathrm{supp}(\boldsymbol{b})$ and $\mathrm{supp}(\boldsymbol{h}) = \mathrm{supp}(\boldsymbol{b})$. The computational cost for perturbative wave function coefficient $\boldsymbol{d}$ only remains a few arithmetic operations except for the first evaluation of $\boldsymbol{h}$.

In addition to the reuse of calculation of $\boldsymbol{d}$, we can avoid re-evaluating diagonal entries during the evaluation of $H_{:,i^{(l+1)}}$. Furthermore, the diagonal entries of the Hamiltonian can also be reused in the linesearch, which solves a cubic equation and requires the information on diagonal entries of the Hamiltonian. With this strategy, the total computational time with the reuse of diagonal entries of the Hamiltonian is only about the same as that of the original CDFCI after some iterations [10h/8h, Cr_2]. The extra computation is mainly due to the first evaluation of $\boldsymbol{h}$. The additional memory cost is the third required vector to be stored in the main memory.

Finally, we focus on the numerical stability of perturbative energy in the implementation of IP-CDFCI. Because CDFCI updates only one determinant in each iteration and the number of iterations can be explosively large, more than 10^8, the variational energy and perturbative energy are calculated by accumulated quantity, i.e. $\boldsymbol{c}^T\boldsymbol{c}$, $\boldsymbol{c}^T\boldsymbol{H}\boldsymbol{c}$, and the variation of $\boldsymbol{d}$. To avoid pollution of variational energy, CDFCI uses quadruple-precision floating-point for $\boldsymbol{c}^T\boldsymbol{c}$ and $\boldsymbol{c}^T\boldsymbol{H}\boldsymbol{c}$. Similarly, we use quadruple-precision floating-point for perturbative energy.

4. IP-CDFCI ACCURACY CRITERION

The IP-CDFCI algorithm embeds the computation of perturbative energy into the iterative calculation of the variational energy, allowing IP-CDFCI to calculate the latest perturbative energy after each iteration without incurring additional memory cost. Meanwhile, since the memory requirement of IP-CDFCI increases gradually with the iteration process, we can always calculate the "best" variational energy and perturbative energy simultaneously before reaching the current memory limit. On the other hand, the unique algorithm design of IP-CDFCI allows for a large number of iterations (usually 10^4 to 10^8) in a short amount of time, even when computing small systems. As the perturbative energy slowly updates with each iteration, it captures the dynamic correlations of the entire system in a more "sensitive" way. With the increase of the variational space, the dimensionality of the perturbative space shows a tendency to first increase and then decrease, and the absolute value of the perturbative energy continues to decrease. According to perturbation theory, the smaller the perturbation of the Hamiltonian, the more accurate the correction given by perturbation theory, and the closer the total perturbative energy is to the exact value. We expect to use the perturbative energy to estimate the error between the current total perturbative energy and the exact value after the dimensionality of the perturbative space begins to decrease.

As shown in the Figure 3, we calculated the exact ground-state energy (E_{ref}) for the H_2O system—adopting a near-dissociation

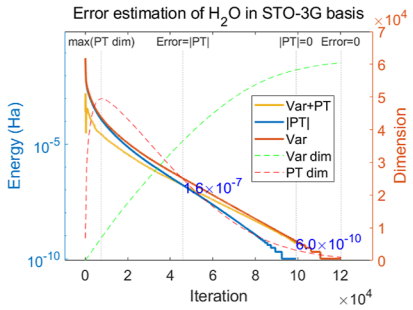

Figure 3. Convergence curve of H_2O system with a small STO-3G basis set of the total perturbative energy error ($E_{\mathrm{Var}} + E_{\mathrm{PT}} - E_{\mathrm{ref}}$) denoted by "Var + PT", the absolute value of the second-order perturbative energy ($|E_{\mathrm{PT}}|$) denoted by "|PT|", and variational energy error ($E_{\mathrm{Var}} - E_{\mathrm{ref}}$) denoted by "Var".

geometry (OH bond length = 1.84345 Å, HOH bond angle = 110.6°)[33] that exhibits strong electron correlation—using a small STO-3G basis set as a reference and plotted the convergence curves of the total perturbative energy error ($E_{\mathrm{Var}} + E_{\mathrm{PT}} - E_{\mathrm{ref}}$), the absolute value of the second-order perturbative energy ($|E_{\mathrm{PT}}|$), and variational energy error ($E_{\mathrm{Var}} - E_{\mathrm{ref}}$) as a function of iteration steps. We used four criteria to distinguish different stages in the convergence process of IP-CDFCI: when the perturbative space dimension is at its maximum (max(PT dim)), when the perturbative total energy error equals the absolute value of the perturbative energy (Error = |PT|), when the absolute value of the perturbative energy equals zero (|PT| = 0), and when the total energy converges to the exact reference energy (Error = 0).

For the scenario where |PT| = 0 and Error = 0, if we want to achieve this level of accuracy, we do not need to use IP-CDFCI calculation. Instead, using the original CDFCI that only calculates the variational energy will result in faster computation with fewer operations. At this stage, the perturbative calculation is entirely an additional expense, so we do not expect to achieve this level of accuracy when using IP-CDFCI calculation.

https://doi.org/10.1021/acs.jctc.6c00103
J. Chem. Theory Comput. 2026, 22, 5005−5019

Table 1. Properties of Test Molecule Systems within cc-pVDZ Basis, MPI and OpenMP Parallelization Were Disabled for All Runs[a]

molecules	electrons	spin orbitals	dimension	HF energy	GS energy
H_2O	10	24	4.53×10^8	−76.0240386	−76.2418600697
C_2	12	28	1.77×10^{10}	−75.4168820	−75.7319604142
N_2	14	28	1.75×10^{11}	−108.9493779	−109.2821730275

[a]Benchmarks were performed on a single node equipped with an Intel Xeon Gold 6226R CPU (2.90 GHz) and 1 TB of memory.

However, it is important to note that when |PT| = 0, it does not necessarily mean that we have reached the exact convergence value of CDFCI. Even after the perturbative energy is lower than the numerical limit, there is still an error of 6.0×10^{-10} in the total energy, which is mainly contributed by the variational energy.

For the scenario where Error = |PT| to |PT| = 0, the total energy error is generally below 1.6×10^{-7}, which is a high level of computational accuracy (and far higher than chemical accuracy). As the number of iterations increases, the absolute value of the perturbative decreases from 1.6×10^{-7} to 0, while the total energy error decreases from 1.6×10^{-7} to 6.0×10^{-10}. In other words, if we use the absolute value of the perturbative instead of the estimated total energy error at this stage, the approximation error introduced will increase from 0 to 6.0×10^{-10} as the iteration progresses. Using the absolute value of the perturbative to replace the total energy error at this stage may overestimate it by up to 6.0×10^{-10}, which is usually not expected in IP-CDFCI calculations. However, plotting the |PT| curve only requires information on the current number of iterations, while plotting the accurate Error curve requires the total energy information at the Error = 0 position, which is difficult to achieve in larger or medium-sized systems.

For the scenario where |PT| = max(PT dim) to Error = |PT|, the total energy error is between 2.7×10^{-5} and 1.6×10^{-7}, while the absolute value of the perturbative is between 1.2×10^{-4} and 1.6×10^{-7}. At this stage, the total energy error has basically reached chemical accuracy, and with increasing iteration, it gradually improves to the level of 1.6×10^{-7}. If we use the absolute value of the perturbative instead of the total energy error, and observe that the absolute value of the perturbation has already reached chemical accuracy, we can assume that the actual accuracy has reached a level 1 order of magnitude higher than chemical accuracy, and as the absolute value of the perturbative gradually decreases to the "high-precision" range of around 1.6×10^{-7}, it becomes increasingly consistent with the accurate total energy error. This stage is the most critical scenario in practical calculations, where we hope to know when we have achieved the lowest acceptable chemical accuracy as soon as possible, while also achieving high precision that is both numerically reliable and above chemical accuracy (such as at the level of 1.6×10^{-7}) using the absolute value of the perturbation to approximate the actual accuracy is very reliable.

For the scenario from the beginning of the calculation to max(PT dim), a considerable portion of the correlated effects in the system is contributed by static correlation. As CDFCI continuously seeks the most important determinant configurations and adds them to the variational space, the perturbative space rapidly expands. At this point, the static and dynamic correlations in the system are coupled, and the perturbation theory energy cannot accurately capture the dynamic correlation information. Therefore, there is significant oscillation in the total energy error at the beginning of the calculation. As the variational space gradually captures the most important physical information from the determinant configurations and the perturbative space reaches its saturation point at max(PT dim), most of the static correlation information in the system is incorporated into the variational space for processing, and the perturbative method is used to handle the dynamic correlation information. The iterative process continues to incorporate lower priority determinant configurations in the perturbative space into the variational space to achieve higher computational accuracy and smaller perturbative space.

Based on the above analysis, we recommend using the original CDFCI that does not include perturbative calculations if higher than 10^{-8} accuracy is desired. When the absolute value of the perturbative energy is near chemical accuracy, the true accuracy can be assumed to be 1 order of magnitude lower than the current absolute value of the perturbative energy. When the absolute value of the perturbative energy is between chemical accuracy and 10^{-8} or higher, the absolute value of the perturbative energy can be used as an approximation of the actual total energy error. The error introduced by this approximation is usually half an order of magnitude up or down from the absolute value of the perturbative energy.

It is also worth noting that when performing IP-CDFCI calculations, regardless of whether the perturbative energy absolute value is used to estimate the error or not, the calculation result should be ensured to be in the stage where the perturbative space begins to decrease.

Here, we wish to articulate the following perspective: while the perturbative total energy provided by IP-CDFCI is not a strictly variational energy in the formal sense (i.e., it does not guarantee an upper bound on the ground-state energy), it exhibits variational-like convergence behavior under specific conditions. As depicted in Figure 3, after the perturbative space ceases to expand (reaching its maximum dimension), the total energy (variational + perturbative) converges robustly toward the accurate FCI energy in a monotonic manner—analogous to the convergence characteristic of variational methods. This behavior arises from the deep coupling between the variational and perturbative iterations in IP-CDFCI: the variational space continuously absorbs critical determinants carrying dominant correlation effects, while the perturbative space only corrects residual dynamic correlation, leading to stable and monotonic convergence of the total energy. We can anticipate that, following the cessation of further expansion in the perturbation space, the perturbative total energy will not yield energy estimates higher than the true ground-state energy during the convergence process. Simultaneously, with the introduction of the compression parameter ε, the objective of the perturbation correction energy is the eigen energy of the ground state in the restricted supp($\boldsymbol{b}$) space. We expect the uncertainty introduced by second-order perturbation theory in providing accurate energy estimates to be sufficiently weak in the current uncompressed scenario. Additionally, this perturbative uncertainty is expected to be significantly weaker compared to

https://doi.org/10.1021/acs.jctc.6c00103
J. Chem. Theory Comput. 2026, 22, 5005−5019

Table 2. Convergence of Energy of H_2O[a]

					IP-CDFCI	
algorithm	parameter	energy	error	time (s)	time (s)	ratio
IP-CDFCI	$\epsilon = 0$	−76.24061621	1.2×10^{-3}	8.76		
		−76.24176018	1.0×10^{-4}	59.63		
		−76.24185007	1.0×10^{-5}	320.97		
		−76.24185907	1.0×10^{-6}	1490.9		
		−76.24185997	1.0×10^{-7}	5652.4		
		−76.24186006	1.0×10^{-8}	15,340		
CDFCI	$\epsilon = 0$	−76.24085600	1.0×10^{-3}	41.36	8.76	4.72×
		−76.24176012	1.0×10^{-4}	204.53	59.63	3.43×
		−76.24185007	1.0×10^{-5}	952.82	320.97	2.96×
		−76.24185907	1.0×10^{-6}	3194.3	1490.9	2.14×
		−76.24185997	1.0×10^{-7}	8371.6	5652.4	1.48×
		−76.24186006	1.0×10^{-8}	17,965	15,340	1.17×
HCI	$\epsilon_1 = 1.0 \times 10^{-4}$	−76.24128914	5.7×10^{-4}	115.51	9.66	11.95×
	$\epsilon_1 = 2.0 \times 10^{-5}$	−76.24175335	1.0×10^{-4}	517.74	56.81	9.11×
	$\epsilon_1 = 1.0 \times 10^{-5}$	−76.24181088	4.9×10^{-5}	889.67	99.22	8.96×
	$\epsilon_1 = 5.0 \times 10^{-5}$	−76.24184017	2.0×10^{-5}	1706.6	191.08	8.93×
DMRG	max $M = 500$	−76.24182145	3.8×10^{-5}	2354.4	117.59	20.02×
	max $M = 1000$	−76.24185639	3.6×10^{-6}	3954.8	650.07	6.08×
	max $M = 2000$	−76.24185984	2.3×10^{-7}	9003.8	3573.8	2.51×
	max $M = 4000$	−76.24186006	9.7×10^{-9}	23,618	15,527	1.52×

[a]The tests have been conducted on a machine with an Intel Xeon Gold 6226R CPU @ 2.90 GHz and 1TB of memory.

the difference between the ground-state energy in the compressed and uncompressed scenarios.

5. BENCHMARKS OF IP-CDFCI

To assess the performance of IP-CDFCI algorithm, we conducted tests on three molecules exhibiting varying correlation strengths: H_2O with OH bond length of 1.84345 Å and HOH bond angle of 110.6°,[23,33] C_2 with a bond length of 1.24253 Å,[11,34] and N_2 with a bond length of 2.118 Å.[35] The FCI Hilbert space dimension N_{FCI} is determined exclusively by the number of electrons and the choice of one-electron basis set (cc-pVDZ in this work), increasing in the order H_2O (4.53×10^8) < C_2 (1.77×10^{10}) < N_2 (1.75×10^{11}) with the number of electrons.

Table 1 summarizes the properties of these systems, with reference ground state energies precisely calculated using IP-CDFCI. The chosen basis sets for all three molecules are full-electron cc-pVDZ. Table 1 also provides specific details about each computational system, including the number of spin orbitals, number of electrons, and FCI Hilbert space dimension. To compare the performance of different algorithms, we employ the IP-CDFCI energy obtained from extensive computations as the accurate ground state energy. The parameters in the Hamiltonian are derived from the FCIDUMP format file generated from restricted HF calculations in the Psi4 software.[36]

The implementation of perturbative CDFCI is detailed in Implementation section. The original version of Dice is used for HCI,[11] while Block2,[37−40] a widely adopted version, is employed for DMRG. The compilation of IP-CDFCI, original CDFCI,[15] and Dice utilizes the Intel compiler version 2022.0.2 with the −O3 option, while Block2 is installed through pip, utilizing intel-openmp-2021.4.0, and mkl-2021.4.0.

It should be noted that MPI and OpenMP support have been disabled for all programs in this section. The tests have been conducted on a machine with an Intel Xeon Gold 6226R CPU @ 2.90 GHz and 1TB of memory. For all algorithms, the Hartree−Fock state is adopted as the initial wave function. The specific parameters for IP-CDFCI, original CDFCI, HCI, and DMRG will be explicitly mentioned later. The values of ϵ_1 and max M are varied for HCI and DMRG, respectively, while any unspecified parameters are set to their default values. Notably, for CDFCI, HCI, and DMRG algorithms, the reported energy does not involve any perturbation or extrapolation. This choice is motivated by two key considerations: first, the perturbative space in our framework is confined to a compressed subspace (not the true full FCI perturbative space), making direct comparison with standard PT-augmented methods inappropriate; second, deterministic perturbative corrections for HCI are computationally prohibitive for the systems studied here, while publicly available DMRG implementations lack integrated perturbative modules, precluding a fair and consistent comparison with DMRG + PT. Additionally, we only adopted a single compression parameter ϵ for the perturbative calculations, as its impact on accuracy is consistent with that in the original CDFCI (as comprehensively analyzed in the original CDFCI work), rendering systematic variation unnecessary for the benchmarks presented herein.[15]

The IP-CDFCI method incorporates the perturbation energy calculation within the variational iteration process, rather than treating it as a postprocessing step after the variational stage. This unique feature allows IP-CDFCI to assess the variational space during iterations. Consequently, we are conducting a performance comparison of IP-CDFCI with variational CDFCI, variational HCI, and variational DMRG algorithms.

In this section, we perform a sequence of benchmark tests to demonstrate the efficiency of IP-CDFCI. We compare the performance of IP-CDFCI, Heat-bath CI (HCI), and DMRG on H_2O, C_2, and N_2 under cc-pVDZ basis. All of the reported energies are in Hartree (Ha).

5.1. H_2O Molecule

For the H_2O molecule, we report the key parameters, computed ground state energies, calculation precision, and computation time of each algorithm in Table 2. Additionally, we have

https://doi.org/10.1021/acs.jctc.6c00103
J. Chem. Theory Comput. 2026, 22, 5005−5019

depicted the graph illustrating the relationship between computation precision and computation time in Figure 4.

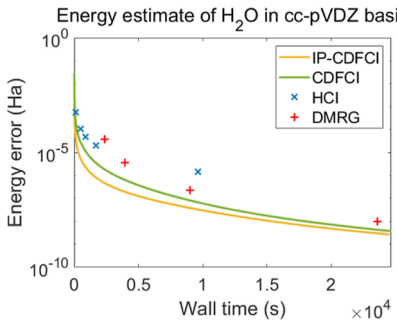

Figure 4. Convergence of ground state energy of H_2O against wall clock time. Each point or curve represents one test as in Table 2.

From the Table 2, it can be observed that each algorithm is capable of calculating ground state energies surpassing chemical accuracy (10^{-3} Ha) within seconds to minutes. Among all variational methods, CDFCI exhibits the fastest computation speed and the lowest variational energy for H_2O. Furthermore, despite conducting tests on a machine with ample memory (1TB), the memory limitation for CDFCI variational energy calculation for the H_2O molecule remains within 32 GB.

In the case of IP-CDFCI calculations, it begins at the same starting point as the variational CDFCI (Hartree−Fock energy) and rapidly obtains higher computation precision compared to CDFCI during the initial calculation phase. Subsequently, after prolonged iterative calculations, IP-CDFCI converges toward the variational CDFCI energy. This trend aligns with the variation of the perturbative space $\mathcal{P}$ as discussed in the preceding section. In CDFCI variational calculations, both static and dynamic correlation effects are treated equivalently. As the variational space $\mathcal{V}$ gradually expands until the perturbative space $\mathcal{P}$ is compressed to zero, typically occurring in the latter stages of lengthy variational iterations, all static and dynamic correlation effects are precisely incorporated into the variational energy. This corresponds to the stage where IP-CDFCI and CDFCI overlap at extremely high precision. However, before this convergence, IP-CDFCI consistently captures a portion of correlation effects "in advance" outside the variational space and processes them using perturbation theory. It should be noted that during the early stages of computation, this part of correlation effects treated with perturbation theory may include both dynamic and static correlation effects. Static correlation effects must be precisely treated through the variational process. As analyzed in the preceding section, this early inappropriate treatment usually occurs during the stage when the perturbative space enlarges, and after several iterations, these configurations that predominantly contribute to static correlation effects are quickly incorporated into the variational space. Therefore, IP-CDFCI achieves a more "economical" way to calculate lower ground state energies. In the H_2O molecular system, within the range from chemical accuracy to higher precision, IP-CDFCI achieves an accuracy level approximately an order of magnitude higher than CDFCI for the same computation time.

From the Table 2, we can also observe that for CDFCI, HCI, and DMRG, the speed advantage of IP-CDFCI in reaching the same precision decreases as the variational energy precision improves. Compared to variational CDFCI, IP-CDFCI achieves chemical accuracy nearly five times faster, while reaching the high precision of 10^{-8} takes approximately a similar amount of time as variational CDFCI. HCI is more efficient in computation compared to DMRG but can not reach higher precision due to more computational memory requirement. On the other hand, DMRG achieves higher precision at a speed almost comparable to CDFCI.

Table 3. Convergence of Energy of C_2[a]

					IP-CDFCI	
algorithm	parameter	energy	error	time (s)	time (s)	ratio
IP-CDFCI	$\varepsilon = 3.0 \times 10^{-8}$	−75.72314608	1.0×10^{-2}	31		
		−75.73096437	1.0×10^{-3}	69.5		
		−75.73186020	1.0×10^{-4}	309.66		
		−75.73195041	1.0×10^{-5}	1595		
		−75.73195941	1.0×10^{-6}	7155.3		
		−75.73196031	1.0×10^{-7}	26,061		
		−75.73196040	1.0×10^{-8}	69,133		
CDFCI	$\varepsilon = 3.0 \times 10^{-8}$	−75.73095910	1.0×10^{-3}	149.38	69.5	2.14×
		−75.73186039	1.0×10^{-4}	833.71	309.66	2.69×
		−75.73195041	1.0×10^{-5}	4092.9	1595	2.56×
		−75.73195941	1.0×10^{-6}	16,254	7155.3	2.27×
		−75.73196031	1.0×10^{-7}	51,240	26,066	1.96×
		−75.73196040	1.0×10^{-8}	11,566	68,951	1.67×
HCI	$\varepsilon_1 = 1.0 \times 10^{-4}$	−75.73053614	1.4×10^{-3}	159.02	56.29	2.82×
	$\varepsilon_1 = 2.0 \times 10^{-5}$	−75.73171295	2.4×10^{-4}	1072.8	165.09	6.49×
	$\varepsilon_1 = 1.0 \times 10^{-5}$	−75.73185411	1.0×10^{-4}	1722.6	297.5	5.79×
	$\varepsilon_1 = 5.0 \times 10^{-5}$	−75.73191696	4.3×10^{-5}	3510.5	571.51	6.14×
DMRG	max M = 500	−75.73111599	8.4×10^{-4}	2341.5	75.91	30.84×
	max M = 1000	−75.73181638	1.4×10^{-4}	4937.8	240.95	20.49×
	max M = 2000	−75.73193978	2.0×10^{-5}	9186.5	976.79	9.40×
	max M = 4000	−75.73195823	2.1×10^{-6}	17,810	4336	4.10×

[a]The tests have been conducted on a machine with an Intel Xeon Gold 6226R CPU @ 2.90 GHz and 1TB of memory.

https://doi.org/10.1021/acs.jctc.6c00103
J. Chem. Theory Comput. 2026, 22, 5005−5019

5.2. C_2 Molecule

The computational results for the C_2 molecule are presented in Table 3 and Figure 5. Similar to the H_2O system, all methods can

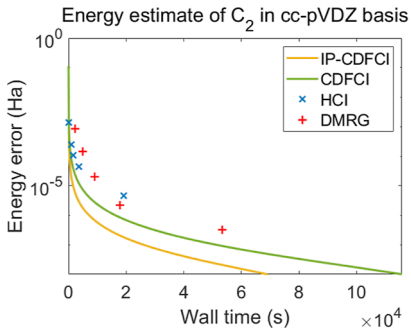

Figure 5. Convergence of ground state energy of C_2 against wall clock time. Each point or curve represents one test as in Table 3.

achieve precision above chemical accuracy within a few minutes. CDFCI remains the fastest among the variational algorithms. For the C_2 molecule, we constrain the computational memory of CDFCI not to exceed 64 GB throughout the calculation. Although not evident in the graph, we also expect IP-CDFCI to converge toward the variational CDFCI energy at high precision. Above the range displayed in the graph, IP-CDFCI can achieve an accuracy level approximately an order of magnitude higher than variational CDFCI for the same computational time. Therefore, as the correlation strength increases, in the case of C_2 compared to the H_2O system, IP-CDFCI can still obtain as many "important" dominant static correlation determinants in the variational space as possible and efficiently capture effective dynamic correlation determinants in the perturbative space, resulting in significantly improved computational efficiency and precision. HCI can still strike a balance between computational precision and efficiency in systems with stronger correlations, but it remains problematic due to its substantial memory requirements. Under higher precision demands, the growth rate of memory requirements also accelerates. In systems with moderate correlation strength like C_2, DMRG can compute higher precision variational energies while maintaining relatively minimal increases in memory requirements. However, compared to HCI, the computation time will be longer.

5.3. N_2 Molecule

In the N_2 molecular system, due to the formation of a triple chemical bond between the two N atoms, the system exhibits stronger electron correlation effects, resulting in a larger FCI Hilbert space dimension. The computational results of each algorithm are presented in Table 4 and Figure 6. It can be

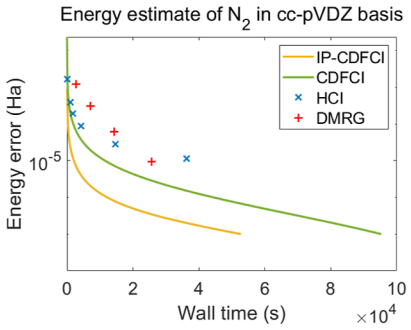

Figure 6. Convergence of ground state energy of N_2 against wall clock time. Each point or curve represents one test as in Table 4.

observed that IP-CDFCI, CDFCI, and HCI can still rapidly achieve accuracy above chemical accuracy. In the medium precision range, HCI is nearly as efficient as variational CDFCI. However, the stronger static correlation effects in the system require a larger number of determinant configurations for HCI to simulate, making it more challenging for HCI to achieve

Table 4. Convergence of Energy of N_2[a]

					IP-CDFCI	
algorithm	parameter	energy	error	time (s)	time (s)	ratio
IP-CDFCI	$\varepsilon = 5.0 \times 10^{-7}$	−109.2812842	8.8×10^{-4}	38.95		
		−109.2820725	1.0×10^{-4}	278.32		
		−109.2821630	1.0×10^{-5}	2076.8		
		−109.2821720	1.0×10^{-6}	12,157		
		−109.2821729	1.0×10^{-7}	52,714		
		−109.2821730	1.0×10^{-8}	99,642		
CDFCI	$\varepsilon = 5.0 \times 10^{-7}$	−109.2811699	1.0×10^{-3}	201.26	38.95	5.16×
		−109.2820731	1.0×10^{-4}	1896.1	278.32	6.81×
		−109.2821630	1.0×10^{-5}	11,494	2076.8	5.53×
		−109.2821720	1.0×10^{-6}	44,366	12,157	3.64×
		−109.2821729	1.0×10^{-7}	95,248	52,714	1.80×
		−109.2821730	1.0×10^{-8}	12,158	99,642	1.22×
HCI	$\varepsilon_1 = 1.0 \times 10^{-4}$	−109.2805259	1.6×10^{-3}	185.87	38.95	4.77×
	$\varepsilon_1 = 2.0 \times 10^{-5}$	−109.2817822	3.9×10^{-4}	1025	92.91	11.03×
	$\varepsilon_1 = 1.0 \times 10^{-5}$	−109.2819787	1.9×10^{-4}	1823	174.16	10.46×
	$\varepsilon_1 = 5.0 \times 10^{-6}$	−109.2820857	8.7×10^{-5}	4167	309.59	13.46×
DMRG	max M = 500	−109.2809545	1.2×10^{-3}	2666.8	38.95	68.46×
	max M = 1000	−109.2818686	3.0×10^{-4}	7118.7	118.52	60.06×
	max M = 2000	−109.2821112	6.1×10^{-5}	14,359	413.61	34.71×
	max M = 4000	−109.2821635	9.5×10^{-6}	25,660	2164.6	11.85×

[a]The tests have been conducted on a machine with an Intel Xeon Gold 6226R CPU @ 2.90 GHz and 1TB of memory.

https://doi.org/10.1021/acs.jctc.6c00103
J. Chem. Theory Comput. 2026, 22, 5005−5019

higher precision due to the increase in memory requirements. On the other hand, DMRG, benefiting from better memory management, can still compute higher precision variational energies. However, the stronger correlation effects result in a longer convergence time. Variational CDFCI reaches a stable linear convergence process after achieving a precision of 10^{-5} at the beginning of the calculation, and IP-CDFCI exhibits a very similar linear convergence process after achieving a precision of 10^{-6} in a shorter time. Similarly, we expect that after longer computations, IP-CDFCI and variational CDFCI will converge to the same ground state energy, as demonstrated in the H_2O system. For the N_2 system with stronger correlation effects due to the triple bond, compared to IP-CDFCI and variational CDFCI, HCI is difficult to calculate higher precision variational energies due to the rapid increase in memory requirements. Although DMRG can obtain more accurate ground state energies with limited memory, the computation time becomes excessively long. In contrast, the IP-CDFCI and variational CDFCI methods exhibit stable performance across systems with different correlation strengths, offering lower memory requirements and higher computational efficiency.

6. APPLICATIONS OF CDFCI + PT

Currently, our IP-CDFCI code only supports single-threaded computations, which makes it time-prohibitive for large molecular systems. Since the original variational CDFCI can be accelerated using OpenMP, we employ a variational-perturbation decoupled, OpenMP-parallelized CDFCI + PT to calculate the ground-state energy of the chromium dimer system. In this section, the CDFCI + PT is compiled using GCC on Intel(R) Xeon(R) Gold 6342 CPU @ 2.80 GHz with 4096 GB of RAM. All calculations were performed using 48 OpenMP threads. To fully utilize the advantages of CDFCI + PT, we did not employ a fully converged variational wave function and energy. Instead, we set a relatively aggressive compression parameter and limited the number of iterations in the variational stage to prevent the perturbative space from excessively expanding.

7. ALL ELECTRON CHROMIUM DIMER CALCULATION

The chromium dimer is a classic example of a strongly correlated system where traditional single-reference computational methods often fail to yield qualitatively correct results.[11,22,41] We used CDFCI + PT with the Ahlrichs VDZ basis set to calculate the all-electron molecule at a bond length of r = 1.5 Å. The Hartree−Fock (HF) energy of the system is −2085.5729707893 Ha. The system contains 48 electrons and 84 spin orbitals, resulting in a FCI space of approximately 10^{23}. The parameters in the FCI Hamiltonian are derived from the FCIDUMP format file generated from restricted HF calculations in the Psi4 software.[36] Various methods, including DMRG,[22] SHCI,[11] and our variational CDFCI algorithm,[15] have been applied to this problem. The Table 5 summarizes all relevant results,[11,15,22] including our CDFCI + PT findings and results from the literature, all reported energies do not include extrapolated energy unless otherwise specified. After 24 h of computation, the variational space dimension $|\mathcal{V}|$ reached 2.8×10^8, while the perturbative space dimension $|\mathcal{P}|$ reached 2.6×10^{10}. After 84 h of computation, the variational space dimension $|\mathcal{V}|$ reached 9.5×10^8, while the perturbative space dimension $|\mathcal{P}|$ reached 4.0×10^{10}. These trends are clearly illustrated in Figure 7. If we take the extrapolated DMRG energy as the reference value, CDFCI + PT achieves chemical accuracy, with precision second only to the extrapolated DMRG results. Given that CDFCI + PT offers superior memory management, under identical memory constraints, SHCI can only store submatrices with a limited number of determinants in memory, which is insufficient for achieving higher accuracy in the variational stage. In contrast, CDFCI + PT can store a larger number of determinants and perturbative space elements, thereby enabling higher accuracy in the perturbative energy calculations.

Table 5. Comparison of Various Computational Methods, Showing Correlation Energies Calculated by Variational Energies and Final Perturbative Energies for Chromium Dimer[a]

method	$\Delta E_{\text{var.}}$	ΔE_{PT}
CDFCI + PT	−870.6	−871.3
SHCI	−811.0	−871.1
DMRG	−870.4	
CCSD(T)	−849.3	
CCSDTQ	−857.3	
DMRG (extrapolated)	−871.8	

[a]The energy unit is mHa.

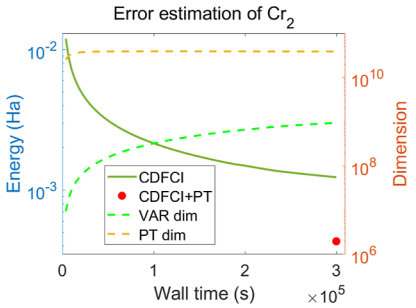

Figure 7. Error estimation curves for the Cr_2 system: the energy error of the CDFCI calculation ($E_{\text{CDFCI}} - E_{\text{ref}}$) is denoted by "CDFCI", where E_{ref} refers to the extrapolated energy from the DMGR method. The final CDFCI + PT corrected energy point is marked by the red dot "CDFCI + PT", the dimension of the variational space ($|\mathcal{V}|$) is denoted by "VAR dim", and the dimension of the perturbative space ($|\mathcal{P}|$) is denoted by "PT dim".

8. CONCLUSION AND OUTLOOK

In this work, we introduced two perturbative extensions of the original CDFCI method, namely CDFCI + PT and IP-CDFCI. The CDFCI + PT approach further refines the variational energy by leveraging perturbation theory, while the IP-CDFCI method improves efficiency by avoiding the evaluation of excessively large perturbative spaces and capturing information from the variational stage. By employing efficient memory management strategies, including the use of sparse vectors and hash tables, as well as quadruple-precision floating-point arithmetic, we significantly enhanced the numerical stability and computational efficiency of our methods. We demonstrated the effectiveness of both single-threaded IP-CDFCI and multithreaded CDFCI + PT through calculations on molecular benchmarks. Our results show that these methods can achieve high accuracy and computational efficiency, making them valuable tools for the study of complex molecular systems. The full source code for CDFCI/CDFCI + PT/IP-CDFCI will be open-sourced on GitHub (https://github.com/quan-tum/CDFCI).

https://doi.org/10.1021/acs.jctc.6c00103
J. Chem. Theory Comput. 2026, 22, 5005−5019

Looking ahead, several promising directions for future work can be explored. First, improving the parallelization efficiency of CDFCI + PT and IP-CDFCI across larger computational platforms could further enhance performance for larger molecular systems. We are already investigating the two-step strategy (performing large-scale variational CDFCI calculations followed by independent perturbative corrections) to address memory limitations associated with storing determinants in the perturbative space, which aligns with our long-term goal of expanding the applicability of CDFCI to larger strongly correlated systems. Additionally, incorporating more advanced techniques for memory management and data storage, such as adaptive sparse representations, may allow for even greater scalability. Another important avenue for exploration involves extending the applicability of these methods to excited states and relativistic systems, where electron correlation effects are particularly challenging to capture. Finally, future research should explore hybrid approaches that combine CDFCI with other quantum chemistry methods to further improve the accuracy and applicability of these perturbative techniques across a broader range of chemical systems.

AUTHOR INFORMATION

Corresponding Authors

Yingzhou Li − *School of Mathematical Sciences, Fudan University, Shanghai 200433, China;* orcid.org/0000-0003-1852-3750; Email: yingzhouli@fudan.edu.cn

Wei Hu − *State Key Laboratory of Precision and Intelligent Chemistry, and Anhui Center for Applied Mathematics, University of Science and Technology of China, Hefei, Anhui 230026, China;* orcid.org/0000-0001-9629-2121; Email: whuustc@ustc.edu.cn

Authors

Zhenlin Zhang − *School of Emerging Technology, Hefei National Research Center for Physical Sciences at the Microscale, and Hefei National Laboratory, University of Science and Technology of China, Hefei, Anhui 230026, China*

Mingyu Qiu − *School of Emerging Technology, Hefei National Research Center for Physical Sciences at the Microscale, and Hefei National Laboratory, University of Science and Technology of China, Hefei, Anhui 230026, China*

Complete contact information is available at: https://pubs.acs.org/10.1021/acs.jctc.6c00103

Author Contributions

‖Z.Z. and M.Q. authors contributed equally.

Notes

The authors declare no competing financial interest.

ACKNOWLEDGMENTS

This work is partly supported by the National Natural Science Foundation of China (42550106, 22503093, 22288201,22173093, 21688102, 12271109), the Innovation Program for Quantum Science and Technology (2021ZD0303306), the Strategic Priority Research Program of the Chinese Academy of Sciences (XDB1170000, XDB0450101), the National Key Research and Development Program of China (2016YFA0200604, 2021YFB0300600), the Anhui Provincial Key Research and Development Program (2022a05020052), the Anhui Province Science and Technology Innovation Project (202423k09020010), the Anhui Initiative in Quantum Information Technologies (AHY090400), the CAS Project for Young Scientists in Basic Research (YSBR-005), by the Hefei National Laboratory for Physical Sciences at the Microscale (KF2020003). We thank the Supercomputing Center of Chinese Academy of Sciences, the Supercomputing Center of USTC, the National Supercomputing Center in Wuxi, and Tianjin, Shanghai, Guangzhou Supercomputing Centers for the computational resources, and the University of Science and Technology of China-Southwest University of Science and Technology Counterpart Cooperation and Development Joint Fund. The AI-driven experiments, simulations and model training were performed on the robotic AI-Scientist platform of Chinese Academy of Sciences.

REFERENCES

(1) Eriksen, J. J. The shape of full configuration interaction to come. *J. Phys. Chem. Lett.* **2021**, *12*, 418−432.

(2) Olsen, J.; Jørgensen, P.; Simons, J. Passing the one-billion limit in full configuration-interaction (FCI) calculations. *Chem. Phys. Lett.* **1990**, *169*, 463−472.

(3) Qiu, M.; Zhang, Z.; Zhang, Z.; Lin, Y.; Li, Y.; Yang, J.; Hu, W. Improved correlation optimized virtual orbital algorithm for plane-wave full configuration interaction calculations. *J. Chem. Theory Comput.* **2025**, *21*, 6559−6571.

(4) Perdew, J. P. Density-functional approximation for the correlation energy of the inhomogeneous electron gas. *Phys. Rev. B* **1986**, *33*, 8822.

(5) Damour, Y.; Véril, M.; Kossoski, F.; Caffarel, M.; Jacquemin, D.; Scemama, A.; Loos, P.-F. Accurate full configuration interaction correlation energy estimates for five-and six-membered rings. *J. Chem. Phys.* **2021**, *155*, 134104.

(6) Huron, B.; Malrieu, J. P.; Rancurel, P. Iterative perturbation calculations of ground and excited state energies from multiconfigurational zeroth-order wavefunctions. *J. Chem. Phys.* **1973**, *58*, 5745−5759.

(7) Schriber, J. B.; Evangelista, F. A. Adaptive configuration interaction for computing challenging electronic excited states with tunable accuracy. *J. Chem. Theory Comput.* **2017**, *13*, 5354−5366.

(8) Tubman, N. M.; Lee, J.; Takeshita, T. Y.; Head-Gordon, M.; Whaley, K. B. A deterministic alternative to the full configuration interaction quantum Monte Carlo method. *J. Chem. Phys.* **2016**, *145*, 044112.

(9) Tubman, N. M.; Freeman, C. D.; Levine, D. S.; Hait, D.; Head-Gordon, M.; Whaley, K. B. Modern approaches to exact diagonalization and selected configuration interaction with the adaptive sampling CI method. *J. Chem. Theory Comput.* **2020**, *16*, 2139−2159.

(10) Greene, S. M.; Webber, R. J.; Weare, J.; Berkelbach, T. C. Improved fast randomized iteration approach to full configuration interaction. *J. Chem. Theory Comput.* **2020**, *16*, 5572−5585.

(11) Holmes, A. A.; Tubman, N. M.; Umrigar, C. J. Heat-bath configuration interaction: an efficient selected configuration interaction algorithm inspired by heat-bath sampling. *J. Chem. Theory Comput.* **2016**, *12*, 3674−3680.

(12) Sharma, S.; Holmes, A. A.; Jeanmairet, G.; Alavi, A.; Umrigar, C. J. Semistochastic heat-bath configuration interaction method: selected configuration interaction with semistochastic perturbation theory. *J. Chem. Theory Comput.* **2017**, *13*, 1595−1604.

(13) Li, J.; Otten, M.; Holmes, A. A.; Sharma, S.; Umrigar, C. J. Fast semistochastic heat-bath configuration interaction. *J. Chem. Phys.* **2018**, *149*, 214110.

(14) Giesbertz, K. J. Are natural orbitals useful for generating an efficient expansion of the wave function? *Chem. Phys. Lett.* **2014**, *591*, 220−226.

(15) Wang, Z.; Li, Y.; Lu, J. Coordinate descent full configuration interaction. *J. Chem. Theory Comput.* **2019**, *15*, 3558−3569.

(16) Wang, Z.; Zhang, Z.; Lu, J.; Li, Y. Coordinate descent full configuration interaction for excited states. *J. Chem. Theory Comput.* **2023**, *19*, 7731−7739.

(17) Wright, S. J. Coordinate descent algorithms. *Math. Program.* **2015**, *151*, 3−34.
(18) Shi, H.-J. M.; Tu, S.; Xu, Y.; Yin, W. A primer on coordinate descent algorithms. *arXiv* **2016**, arXiv:1610.00040.
(19) Levine, D. S.; Hait, D.; Tubman, N. M.; Lehtola, S.; Whaley, K. B.; Head-Gordon, M. CASSCF with extremely large active spaces using the adaptive sampling configuration interaction method. *J. Chem. Theory Comput.* **2020**, *16*, 2340−2354.
(20) White, S. R.; Martin, R. L. Ab initio quantum chemistry using the density matrix renormalization group. *J. Chem. Phys.* **1999**, *110*, 4127−4130.
(21) Chan, G. K.-L.; Sharma, S. The density matrix renormalization group in quantum chemistry. *Annu. Rev. Phys. Chem.* **2011**, *62*, 465−481.
(22) Olivares-Amaya, R.; Hu, W.; Nakatani, N.; Sharma, S.; Yang, J.; Chan, G. K.-L. The ab-initio density matrix renormalization group in practice. *J. Chem. Phys.* **2015**, *142*, 034102.
(23) Booth, G. H.; Thom, A. J. W.; Alavi, A. Fermion monte carlo without fixed nodes: A game of life, death, and annihilation in slater determinant space. *J. Chem. Phys.* **2009**, *131*, 054106.
(24) Booth, G. H.; Grüneis, A.; Kresse, G.; Alavi, A. Towards an exact description of electronic wavefunctions in real solids. *Nature* **2013**, *493*, 365−370.
(25) Lu, J.; Wang, Z. The full configuration interaction quantum monte carlo method through the Lens of Inexact Power Iteration. *SIAM J. Sci. Comput.* **2020**, *42*, B1−B29.
(26) Cleland, D.; Booth, G. H.; Alavi, A. Communications: Survival of the fittest: Accelerating convergence in full configuration-interaction quantum Monte Carlo. *J. Chem. Phys.* **2010**, *132*, 041103.
(27) Li, Y.; Lu, J.; Wang, Z. CoordinateWise descent methods for leading eigenvalue problem. *SIAM J. Sci. Comput.* **2019**, *41*, A2681−A2716.
(28) Li, Y.; Lu, J. Optimal orbital selection for full configuration interaction (OptOrbFCI): pursuing the basis set limit under a budget. *J. Chem. Theory Comput.* **2020**, *16*, 6207−6221.
(29) Bierman, J.; Li, Y.; Lu, J. Qubit count reduction by orthogonally constrained orbital optimization for variational quantum excited-state solvers. *J. Chem. Theory Comput.* **2024**, *20*, 3131−3143.
(30) Bierman, J.; Li, Y.; Lu, J. Improving the accuracy of variational quantum eigensolvers with fewer qubits using orbital optimization. *J. Chem. Theory Comput.* **2023**, *19*, 790−798.
(31) Bylaska, E. J.; Song, D.; Bauman, N. P.; Kowalski, K.; Claudino, D.; Humble, T. S. Quantum solvers for plane-wave hamiltonians: Abridging virtual spaces through the optimization of pairwise correlations. *Front. Chem.* **2021**, *9*, 603019.
(32) Barone, V. Anharmonic vibrational properties by a fully automated second-order perturbative approach. *J. Chem. Phys.* **2005**, *122*, 014108.
(33) Olsen, J.; Jo/rgensen, P.; Koch, H.; Balkova, A.; Bartlett, R. J. Full configuration−interaction and state of the art correlation calculations on water in a valence double-zeta basis with polarization functions. *J. Chem. Phys.* **1996**, *104*, 8007−8015.
(34) Sharma, S.; Alavi, A. Multireference linearized coupled cluster theory for strongly correlated systems using matrix product states. *J. Chem. Phys.* **2015**, *143*, 102815.
(35) Chan, G. K.-L.; Kállay, M.; Gauss, J. State-of-the-art density matrix renormalization group and coupled cluster theory studies of the nitrogen binding curve. *J. Chem. Phys.* **2004**, *121*, 6110−6116.
(36) Parrish, R. M.; et al. Psi4 1.1: An open-source electronic structure program emphasizing automation, advanced libraries, and interoperability. *J. Chem. Theory Comput.* **2017**, *13*, 3185−3197.
(37) Zhai, H.; Larsson, H. R.; Lee, S.; Cui, Z.-H.; Zhu, T.; Sun, C.; Peng, L.; Peng, R.; Liao, K.; Tölle, J.; et al. others Block2: A comprehensive open source framework to develop and apply state-of-the-art DMRG algorithms in electronic structure and beyond. *J. Chem. Phys.* **2023**, *159*, 234801.
(38) Chan, G. K.-L.; Head-Gordon, M. Highly correlated calculations with a polynomial cost algorithm: A study of the density matrix renormalization group. *J. Chem. Phys.* **2002**, *116*, 4462−4476.
(39) Sharma, S.; Chan, G. K.-L. Spin-adapted density matrix renormalization group algorithms for quantum chemistry. *J. Chem. Phys.* **2012**, *136*, 124121.
(40) Wouters, S.; Van Neck, D. The density matrix renormalization group for ab initio quantum chemistry. *Eur. Phys. J. D* **2014**, *68*, 272.
(41) Larsson, H. R.; Zhai, H.; Umrigar, C. J.; Chan, G. K.-L. The chromium dimer: closing a chapter of quantum chemistry. *J. Am. Chem. Soc.* **2022**, *144*, 15932−15937.

https://doi.org/10.1021/acs.jctc.6c00103
J. Chem. Theory Comput. 2026, 22, 5005−5019